Supporting Information

A New Family of Heterometallic Ln^{III} [12-$MC_{Fe^{III}N(shi)}$-4] Complexes: Syntheses, Structures, and Magnetic Properties

Tingting Lou, Hua Yang, Suyuan Zeng, Dacheng Li, Jianmin Dou*

*Corresponding author Tel: +8606358239298. E-mail: dougroup@163.com

School of Chemistry and Chemical Engineering, and Shandong Provincal Key Laboratory of Chemical Energy Storage and Novel Cell Technology, Liaocheng University, Liaocheng, Shangdong 252000, PR China.

Contents:

Figure. S12. Plots of isothermal magnetization *M* vs. *H* for complex **2** at 1.8-8 K (left). Plots of magnetization *M* vs. *H*/*T* for complex **2** at 1-7 T (right).

Figure. S13. Plots of isothermal magnetization *M* vs. *H* for complex **3** at 1.8-8 K (left). Plots of magnetization *M* vs. *H*/*T* for complex **3** at 1-7 T (right).

Figure. S14. Plots of isothermal magnetization *M* vs. *H* for complex **4** at 1.8-8 K (left). Plots of magnetization *M* vs. *H*/*T* for complex **4** at 1-7 T (right).

Table S1. The BVS calculations for complexes **1-4**

Table S2. Selected bond angles for complexes **1–3**

Table S3. The distances between Ln-O for complexes **1–4**

Table S4. The distortion angles of benzoate for complexes **1–4**

Table S5. Fit parameters for the Fe 2p XP spectra of complexes **1-4.**

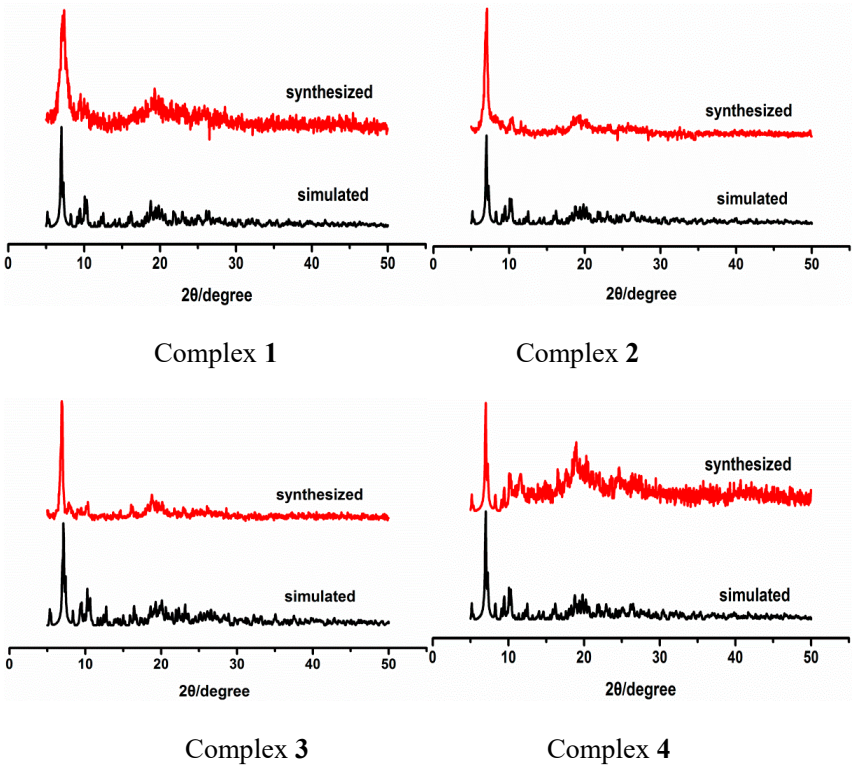

Figure. S1. The experimental XRD pattern of samples and the simulated XRD pattern of single crystal X-ray diffraction data for complexes **1-4**.

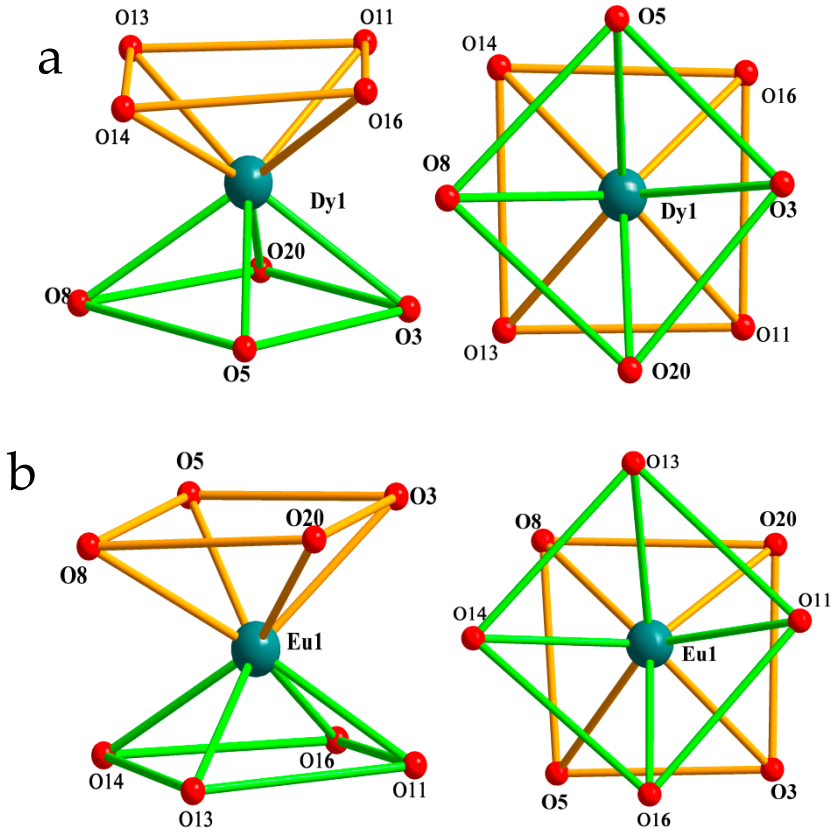

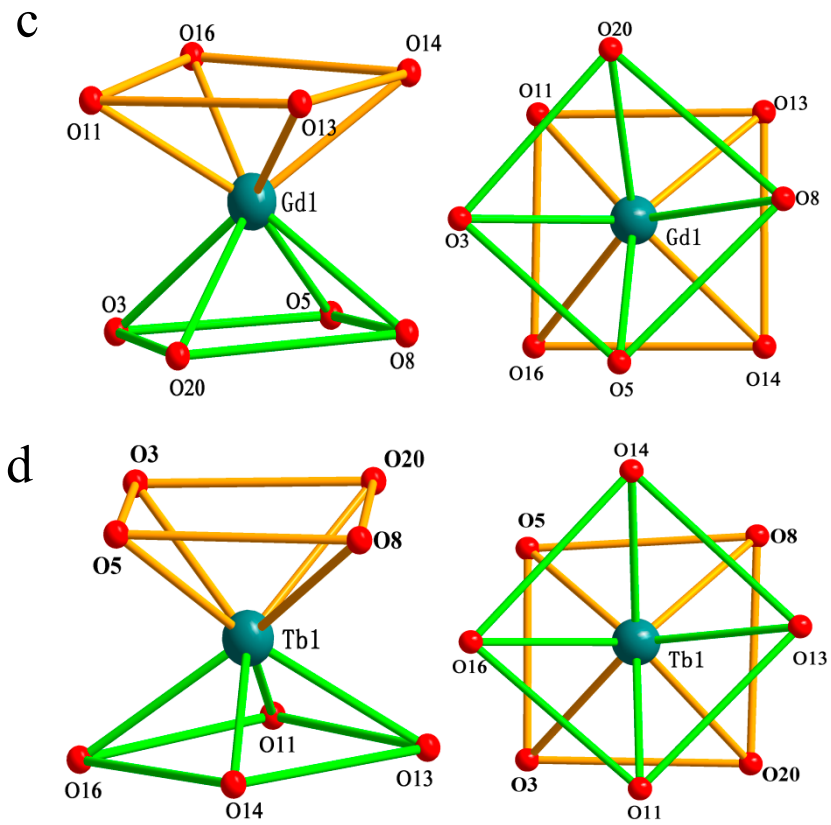

Figure. S2. Distorted square-antiprismatic geometries around Dy1(a), Eu1(b), Gd1(c), Tb1(d)

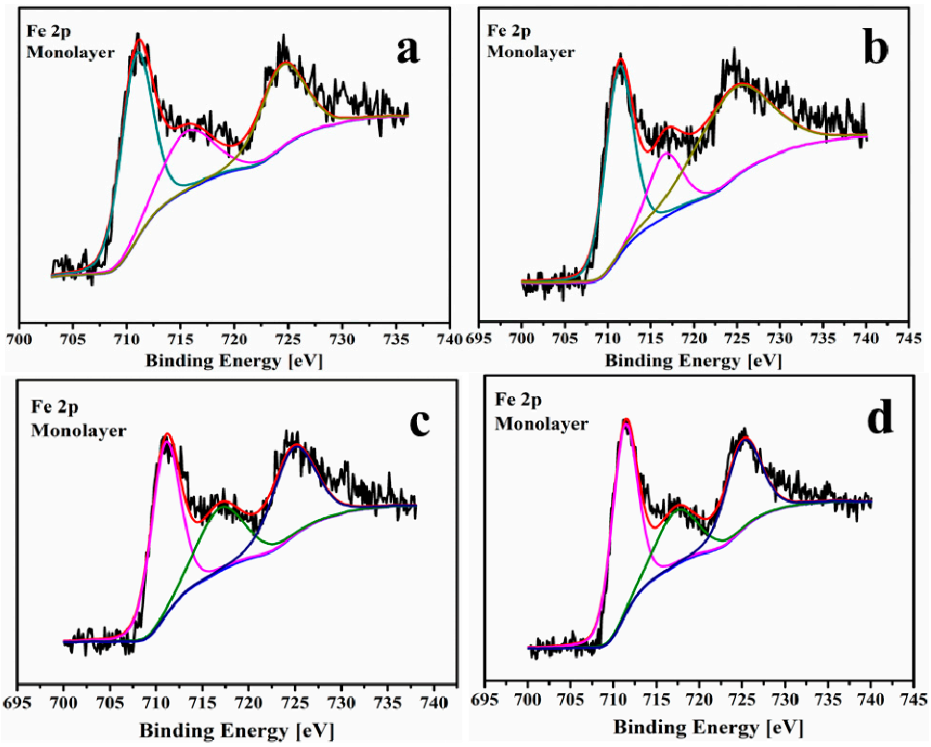

Figure. S3. Fe 2p XP spectras of complexes **1** (a), **2** (b), **3** (c), **4** (d) in monolayers.

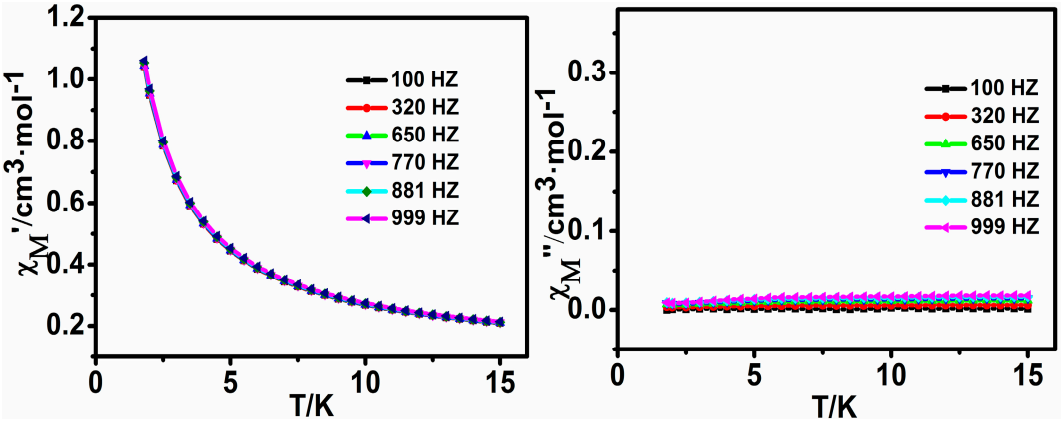

Figure. S4. Temperature dependence of the in-phase (χ'_M) and out-of phase (χ''_M) ac susceptibility signals of complex **1** measured under 2.0 Oe field with a 0 dc field.

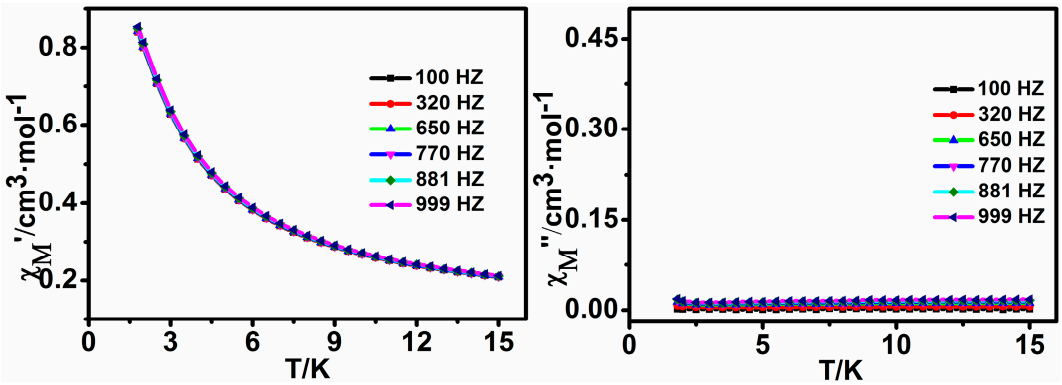

Figure. S5. Temperature dependence of the in-phase (χ'_M) and out-of phase (χ''_M) ac susceptibility signals of complex **1** measured under 2.0 Oe field with a 2000 Oe dc field.

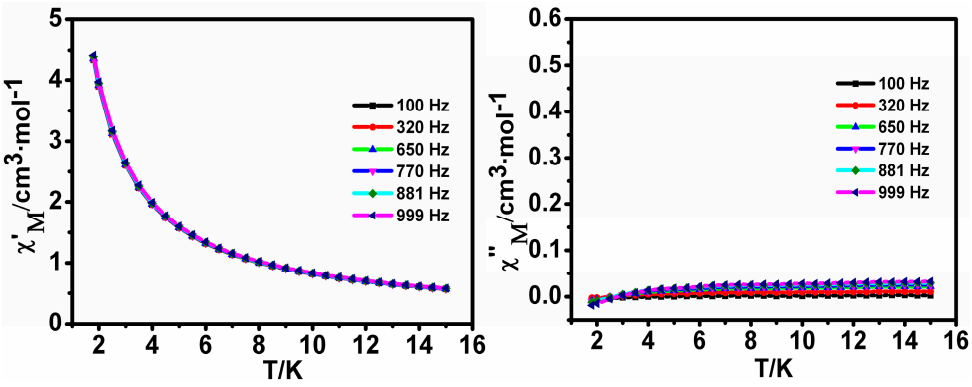

Figure. S6. Temperature dependence of the in-phase (χ'_M) and out-of phase (χ''_M) ac susceptibility signals of complex **2** measured under 2.0 Oe field with a 0 dc field.

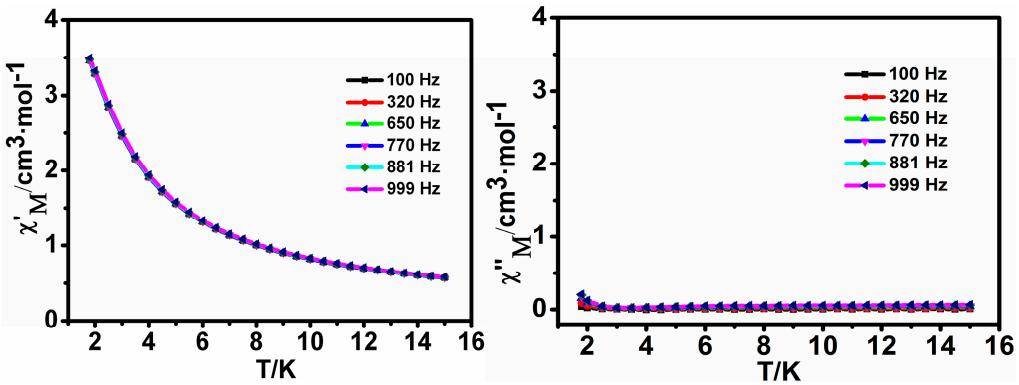

Figure. S7. Temperature dependence of the in-phase (χ'_M) and out-of phase (χ''_M) ac susceptibility signals of complex **2** measured under 2.0 Oe field with a 2000 Oe dc field.

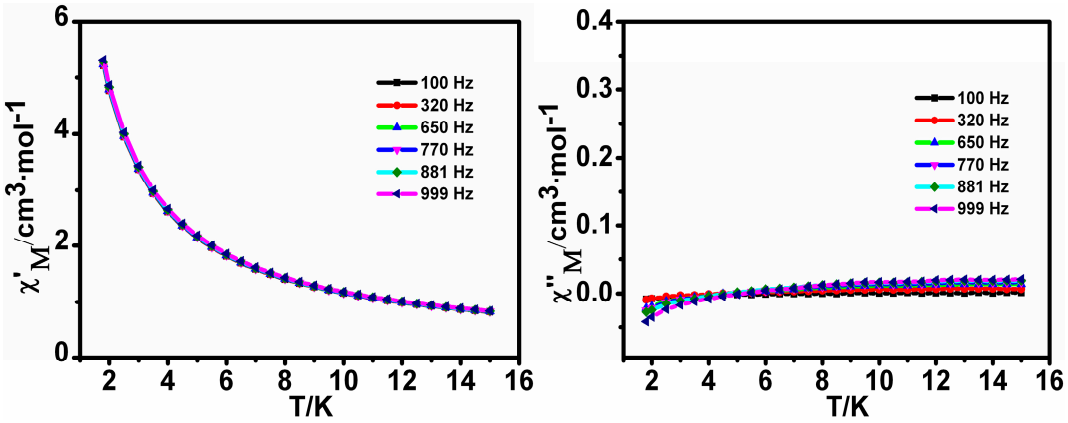

Figure. S8. Temperature dependence of the in-phase (χ'_M) and out-of phase (χ''_M) ac susceptibility signals of complex **3** measured under 2.0 Oe field with a 0 Oe dc field.

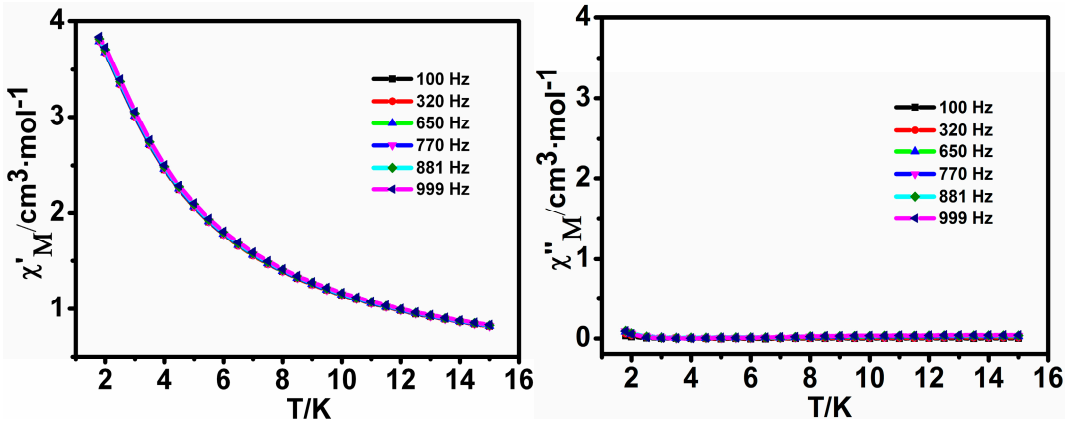

Figure. S9. Temperature dependence of the in-phase (χ'_M) and out-of phase (χ''_M) ac susceptibility signals of complex **3** measured under 2.0 Oe field with a 2000 Oe dc field.

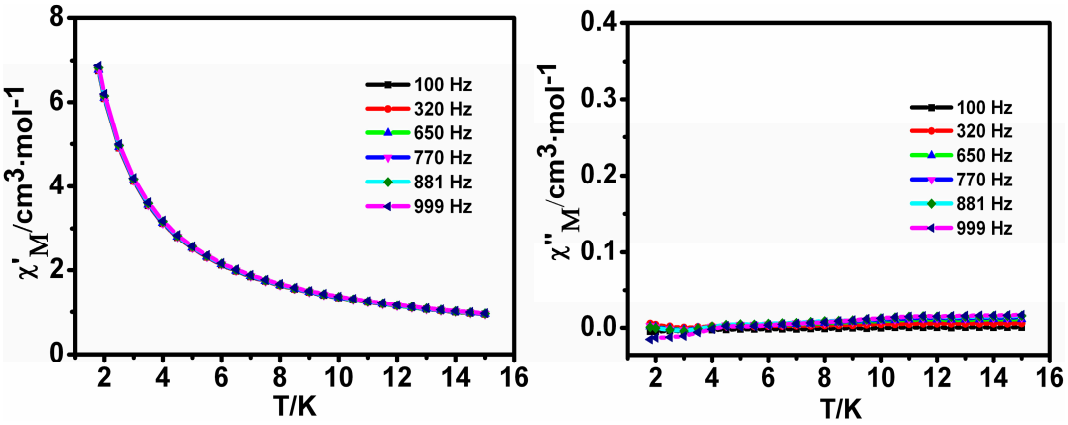

Figure. S10. Temperature dependence of the in-phase (χ'_M) and out-of phase (χ''_M) ac susceptibility signals of complex **4** measured under 2.0 Oe field with a 0 Oe dc field.

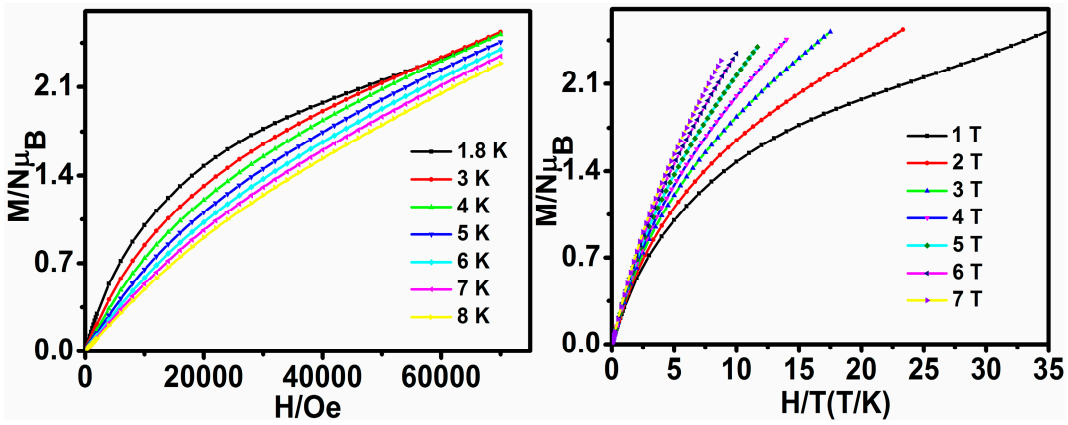

Figure. S11. Plots of isothermal magnetization *M* vs. *H* for complex **1** at 1.8- 8 K (left). Plots of magnetization *M* vs. *H*/*T* for complex **1** at 1-7 T (right).

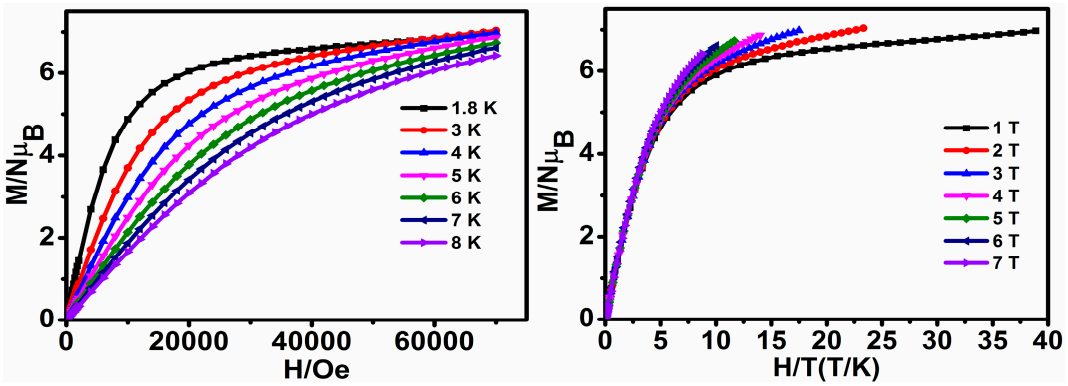

Figure. S12. Plots of isothermal magnetization *M* vs. *H* for complex **2** at 1.8- 8 K (left). Plots of magnetization *M* vs. *H*/*T* for complex **2** at 1-7 T (right).

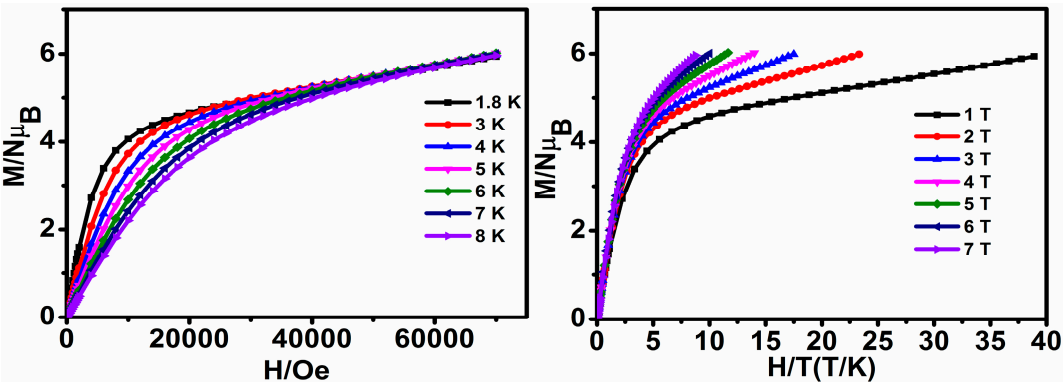

Figure. S13. Plots of isothermal magnetization *M* vs. *H* for complex **3** at 1.8- 8 K (left).

Plots of magnetization *M* vs. *H*/*T* for complex **3** at 1-7 T (right).

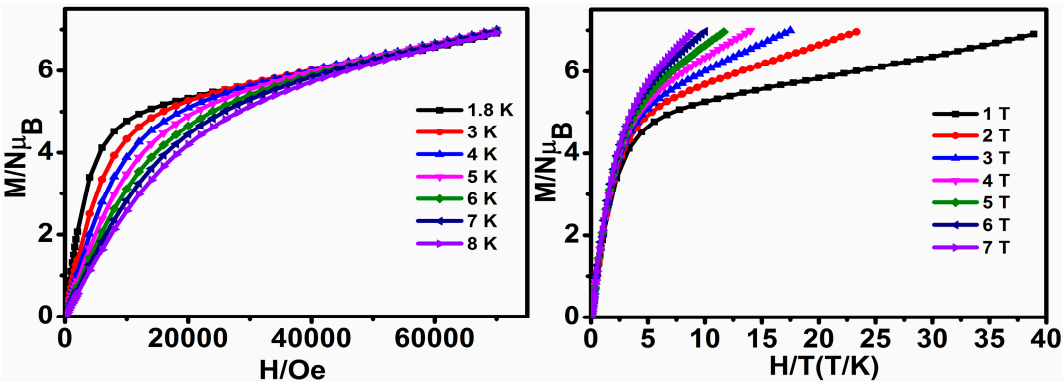

Figure. S14. Plots of isothermal magnetization *M* vs. *H* for complex **4** at 1.8- 8 K (left).

Plots of magnetization *M* vs. *H*/*T* for complex **4** at 1-7 T (right).

Table S1. The BVS calculations for complexes **1-4**

	Complex **1**		Complex **2**		Complex **3**		Complex **4**	
	Fe^{2+}	Fe^{3+}	Fe^{2+}	Fe^{3+}	Fe^{2+}	Fe^{3+}	Fe^{2+}	Fe^{3+}
Fe1	2.87	3.14	2.91	3.18	2.86	3.13	2.86	3.12
Fe2	2.87	3.19	3.02	3.29	2.92	3.19	2.88	3.14
Fe3	2.91	3.18	3.02	3.29	2.89	3.15	2.91	3.17
Fe4	2.87	3.12	2.92	3.19	2.87	3.12	2.85	3.11

Table S2. Selected bond angles for complexes **1–3**

	Complex 1		
O(13)-Eu(1)-O(16) (γ angle)	117.192(155)	O(20)-Eu(1)-O(5) (γ angle)	108.016(129)
α angle (O13, O16)	58.596	α angle (O20, O5)	54.008
O(14)-Eu(1)-O(11) (γ angle)	119.929(160)	O(3)-Eu(1)-O(8) (γ angle)	111.431(144)

α angle (O14, O11)	59.965	α angle (O3, O8)	55.717
Complex 2			
O(13)-Gd(1)-O(16) (γ angle)	115.572(147)	O(20)-Gd(1)-O(5) (γ angle)	107.819(136)
α angle (O13, O16)	57.786	α angle (O20, O5)	53.910
O(14)-Gd(1)-O(11) (γ angle)	118.751(136)	O(3)-Gd(1)-O(8) (γ angle)	112.195(145)
α angle (O14, O11)	59.376	α angle (O3, O8)	56.098
Complex 3			
O(13)-Tb(1)-O(16) (γ angle)	116.910(199)	O(20)-Tb(1)-O(5) (γ angle)	108.693(167)
α angle (O13, O16)	58.455	α angle (O20, O5)	54.347
O(14)-Tb(1)-O(11) (γ angle)	119.210(195)	O(3)-Tb(1)-O(8) (γ angle)	111.314(149)
α angle (O14, O11)	59.605	α angle (O3, O8)	55.657

Table S3. The distances between Ln-O for complexes **1–4**

complex **1**		complex **2**	
Eu(1)-O(11)	2.378(4)	Gd(1)-O(11)	2.361(4)
Eu(1)-O(14)	2.379(4)	Gd(1)-O(14)	2.369(3)
Eu(1)-O(13)	2.381(4)	Gd(1)-O(16)	2.379(3)
Eu(1)-O(5)	2.392(4)	Gd(1)-O(13)	2.382(3)
Eu(1)-O(3)	2.402(4)	Gd(1)-O(5)	2.393(3)
Eu(1)-O(16)	2.410(4)	Gd(1)-O(20)	2.397(3)
Eu(1)-O(20)	2.418(4)	Gd(1)-O(3)	2.415(3)
Eu(1)-O(8)	2.487(4)	Gd(1)-O(8)	2.475(3)
complex **3**		complex **4**	
Tb(1)-O(11)	2.338(5)	Dy(1)-O(11)	2.333(6)
Tb(1)-O(13)	2.359(5)	Dy(1)-O(13)	2.361(5)
Tb(1)-O(14)	2.362(5)	Dy(1)-O(14)	2.366(5)
Tb(1)-O(5)	2.366(5)	Dy(1)-O(5)	2.383(5)
Tb(1)-O(16)	2.381(5)	Dy(1)-O(16)	2.393(5)
Tb(1)-O(3)	2.383(5)	Dy(1)-O(3)	2.399(5)
Tb(1)-O(20)	2.403(5)	Dy(1)-O(20)	2.409(5)
Tb(1)-O(8)	2.458(5)	Dy(1)-O(8)	2.466(5)

Table S4. The distortion angles of benzoate for complexes **1–4**

complex **1**		complex **2**	
$MP_{(Fe1O5Eu)}$-$Mp_{(benzoate)}$	28.766(766)	$MP_{(Fe1O5Gd)}$-$Mp_{(benzoate)}$	30.668(224)
$MP_{(Fe2O3Eu)}$-$Mp_{(benzoate)}$	70.899(226)	$MP_{(Fe2O3Gd)}$-$Mp_{(benzoate)}$	69.105(32)
$MP_{(Fe3O8Eu)}$-$Mp_{(benzoate)}$	76.264(167)	$MP_{(Fe3O8Gd)}$-$Mp_{(benzoate)}$	75.680(275)
$MP_{(Fe4O8Eu)}$-$Mp_{(benzoate)}$	80.728(223)	$MP_{(Fe4O8Gd)}$-$Mp_{(benzoate)}$	79.704(308)
complex **3**		complex **4**	
$MP_{(Fe1O5Tb)}$-$Mp_{(benzoate)}$	30.075(222)	$MP_{(Fe1O5Dy)}$-$Mp_{(benzoate)}$	28.981(225)
$MP_{(Fe2O3Tb)}$-$Mp_{(benzoate)}$	69.874(329)	$MP_{(Fe2O3Dy)}$-$Mp_{(benzoate)}$	70.731(341)
$MP_{(Fe3O8Tb)}$-$Mp_{(benzoate)}$	75.246(242)	$MP_{(Fe3O8Dy)}$-$Mp_{(benzoate)}$	75.634(253)
$MP_{(Fe4O8Tb)}$-$Mp_{(benzoate)}$	79.218(304)	$MP_{(Fe4O8Dy)}$-$Mp_{(benzoate)}$	79.146(309)

Table S5. Fit parameters for the Fe 2p XP spectra of complexes **1-4**.

complex / Binding Energy(eV)	Fe $2p_{3/2}$	Satellite	Fe $2p_{1/2}$
complex **1**	711.11	717.13	724.82
complex **2**	711.50	717.97	725.40
complex **3**	711.10	718.07	725.14
complex **4**	711.49	718.33	725.38